Polym. Bull. (2009) 62:511–524
DOI 10.1007/s00289-008-0031-x

ORIGINAL PAPER

Colloidal Cu nanoparticles/chitosan composite film obtained by microwave heating for food package applications

G. Cárdenas · J. Díaz V. · M. F. Meléndrez · C. Cruzat C. · A. García Cancino

Received: 18 August 2008 / Revised: 8 November 2008 / Accepted: 14 December 2008 /
Published online: 8 January 2009

Abstract In this paper, we describe the preparation and characterization of colloidal Cu nanoparticles/chitosan composite film (composite film) by solution-casting technique with microwave heating. Effects of the incorporation of colloidal Cu nanoparticles on structure, thermal behavior, surface, barrier properties and light transmission of composite film were investigated. The antimicrobial activity of films against *Staphylococcus aureus* and *Salmonella enterica* serovar Typhimurium, were also tested. Incorporation of colloidal Cu nanoparticles on chitosan matrix improved the barrier properties of films, decreasing the oxygen permeability as well as water vapor permeability and increasing the protection against UV light. The composite film was effective in alteration of cell wall and reduction of microbial concentration in the liquid culture for both bacteria tested.

Keywords Colloidal Cu nanoparticles · Chitosan · Microwave heating · Films · Light barrier · Water barrier · Antimicrobial activity

Introduction

Major topic in the synthesis of inorganic–organic materials is the combination of bioactive components. A hybrid material is a material that includes two moieties

G. Cárdenas (✉) · J. Díaz V. · M. F. Meléndrez · C. Cruzat C.
CIPA-Chile, Department of Polymers, Advanced Materials Laboratory,
University of Concepcion, Casilla 160, Chile
e-mail: galocardenas@udec.cl

J. Díaz V.
e-mail: jdiazv@udec.cl

A. García Cancino
Department of Microbiology, Faculty of Biology, University of Concepcion,
Casilla 160, Chile

blended on the molecular scale. Commonly, one of these compounds is inorganic and the other one is organic in nature [1]. Condensation of metal atoms with organic solvents at 77 K is a known technique providing several reactions [2]. Colloidal particles in non-aqueous systems present different properties to bulk material and due to their nanometric size, a large fraction of atoms is localized on the surface, producing unusual properties [3]; that can be used to perform other materials. Chitosan, copolymer of β-(1-4)-2-acetamido-2-deoxy-β-D-glucose and β-(1-4)-2-amine-2-deoxy-β-D-glucose, has focused the attention for its film-forming capacity [4]. Polysaccharides based films have serious problems with their water barrier properties, due to the hydrophilic nature. A determinant factor in the mechanism of water transport through chitosan films is the polymeric matrix and the hydrophilic and electrolytic properties of film-forming solutions. The incorporation of smaller inorganic particles into larger polymers is desirable in order to combine parameters of both materials and improve the physicochemical properties of polymers. Water vapor barrier properties of biopolymer films depend largely on their plasticizer and moisture contents [5, 6]. Several compounds have been incorporated into solution systems in order to increase the hydrophobicity of polysaccharide based films [7, 8]. Recently, we described the preparation of chitosan films by microwave heating [9]; the present paper is an extension of this technique describing the incorporation of colloidal Cu nanoparticles (colloidal Cu nps) in chitosan film-forming solutions and the performance of this composite film depending on their barrier properties.

Experimental

Chitosan (95% deacetylation degree with 400,000 Da) was gently provided by Quitoquímica Co. (Coronel, VIII Región, Chile). All chemicals were analytical grade.

Preparation and characterization of colloidal Cu nanoparticles

A metal atom reactor was used for this purpose [9]. An alumina–tungsten crucible was charged with 50 mg Cu metal (pieces). Gaseous 2-propanol was injected in a ligand inlet tube and attached to neck of the reactor. 2-Propanol was dried with molecular sieves and degasified three times by standard freeze–thaw procedure [10].

The reactor was pumped down to 1×10^{-4} atm and the crucible was heated at 40 A in order to reach the Cu boiling point. A liquid nitrogen filled dewar was placed around the vessel, and Cu and 2-propanol (100 mL) were deposited for 1 h. The matrix was allowed to warm slowly for 1 h under vacuum by removing the dewar full of liquid nitrogen. Upon meltdown, a black-purple colloid was obtained. After the addition of nitrogen up to 1 atm, the colloid was allowed to warm for another 1.5 h, to room temperature. The sol was siphoned into a dark flask under nitrogen and stored at 23 °C in vacuum chamber. The UV–visible absorption spectra of colloidal Cu nps, CS film and their composite film were recorded using a UV–vis spectrophotometer Shimadzu Corp, Kyoto Japan. TEM micrographs were

obtained using a TEM (JEOL–JEM 1200EXII). A drop of colloid was placed on a copper grid previously coated with carbon.

Preparation of films

Chitosan solutions (2% w/v) were prepared by dissolving in acetic acid (1.0%, v/v) with stirring for 13 h, with further filtration through a Schott filter. Colloidal Cu nps were dispersed in chitosan solution (20% v/v) for 48 h in an inert atmosphere (vacuum chamber). Composite solution and chitosan solution (30 mL) were poured in the casting plate and dried for 10 min at full power level, using a Thomas microwave/convection oven (model TH-MO17D, Robert Thomas-Germany, 2,450 MHz) and were left to final dry at atmospheric conditions for 2 h. The heating was carried out one by one and stabilized to room temperature [9]. Films were placed in polystyrene bags, covered with aluminum foil and stored at 20 °C/50% RH.

Analysis techniques

Film thickness was determined with a hand electronic digital micrometer. Shown values are an average of ten measurements. The FTIR spectra were recorded from 4,000 to 100 cm^{-1} on a Nicolet Nexus spectrometer at room temperature (Nicolet Instrument Co., USA). Thermal analysis was performed using a Thermogravimeter Analyzer Perkin Elmer TGA 7. Differential scanning calorimetry (DSC) curves were performed with a Universal V4.3A TA Instruments. The metal content was determined by atomic absorption spectrometry, using a Varian 1475.

Water vapor transmission rate (WVTR) was determined according to ISO 2528 standard method, 1995(E) [11] with WVP correction method [6]. The films with an area of 1.0×10^{-3} m^2 were exposed for 24 h at 20 °C and 50% RH before determination. Films were mounted on cups filled with water. The cups were placed at 90% RH in desiccators ($BaCl_2$ saturated solution). Weight cups were measured at 24 h intervals. Weight loss versus time plots and simple linear regression were used to found the slope and to calculate water vapor transmission rate (WVTR). The WVP of the films was calculated by multiplying the steady state water vapor transmission rate by the average film thickness determined as described above and dividing by the water vapor partial pressure difference across the films. An Ox-Tran® Model 2/61 (Modern Controls Inc., Minneapolis, MN) was used to measure oxygen transmission rates (OTR). Testing was performed at 20 °C in a dry environment (0% RH) and was done in triplicate to get the average mean value. Each film was placed on a stainless steel cell with an open testing area of 5 cm^2. The gas flow rate was fixed at 10 ml/min and the difference in pressure across the film corresponded to atmospheric pressure. OTR values were obtained in cm^3O_2/m^2 day. Oxygen permeability was calculated by dividing O_2 transmission rate by the difference in O_2 partial pressure between both sides of the film (1 atm) and multiplying by the average film thickness measured at 10 random places. Units for OP were cm^3 mm/m^2 day kPa.

Equilibrium moisture content (EMC) was determined according to Pinotti et al. [12]. The weight loss of films was measured upon drying until constant weight at

110 °C (dry sample weight). Equilibrium moisture content (%) was calculated as follows:

$$\text{EMC } (\%) = \left(\frac{\text{Initial sample weight}}{\text{dry sample}} - 1 \right) \times 100 \quad (1)$$

Surface microstructure

For TEM micrographs of composite film, a thin section of the film was made by encapsulating it in an epoxy resin matrix and cutting an 80 nm film at 25 °C using an ultramicrotome Buehler ISOMET equipped with a diamond knife. The thin section of composite film was evaluated using a JEOL-JEM 6380 LV. Atomic force microscopy (AFM) images of composite film and CS film were carried out by using a Capçal STM/AFM Nanoscope Extended Multimode at room temperature conditions. Scanning electron microscopy (SEM) was used to examine representative film surfaces; samples were sputter-coated with gold and scanned using a JEOL-JEM 6380 LV.

Opacity, light transmission and transparency

Opacity was measured according to the method described by Cho and Rhee [13]. Films were cut into rectangles (1.0 × 3.0 cm) and placed in a film holder device. A spectrum of each film was recorded using a spectrophotometer (2,450 UV–vis spectrophotometer Shimadzu Corp, Kyoto, Japan). The area under the absorbance curve from 400 to 800 nm was taken as the opacity of film. It was expressed as absorbance unit (AU) × nm/unit thickness (μm). The opacity measurements were performed at 0, 7, 14, 21 and 28 days of storage at 23 °C in polystyrene bags. Absorbance values were normalized, so that no absorbance scale is given in Fig. 6b. Transparency of films was calculated as follows:

$$\text{Transparency} = \left(\frac{\text{Absorbance (nm OD)}}{\text{Thickness (μm)}} \right) \quad (2)$$

Antimicrobial activity

Two bacterial strains were tested: *Staphylococcus aureus* ATCC 25923 (gram-positive) and *Salmonella enterica* serovar Typhimurium (clinical isolate, Hospital del Trabajador, Concepción, Chile; gram-negative). The test bacteria were grown overnight in sterile Mueller–Hinton Broth (HiMedia Lab., Mumbai, India) at 37 °C under static conditions. An aliquot of 10 μL of the culture was transferred to 30 ml sterile broth. Approximately, 0.060 g of films (8.04 cm^2 surface area) was added to the test flask. The flask was placed in an incubator at 37 °C, leaving the bacteria to grow for 16 h. A standard plate count method on Mueller–Hinton Agar (HiMedia Lab., Mumbai, India) was used to determine the concentration of bacteria able to reproduce. After incubation, fractions of cells were collected by centrifugation (10,835 × *g*, 3 min and 4 °C) and washed three times with sterile nanopure water. Cells were resuspended with nanopure water and 20 μL of bacterial suspension were deposited on copper grids and fixed with 10 μL 1% formaldehyde. Another

fraction of bacterial suspension was fixed at 4 °C for 90 min with 2% glutaraldehyde in 0.1 M sodium phosphate buffer, pH 7.4. Cells were postfixed in 1% OsO_4 for 90 min at 4 °C and stained with 0.25% uranyl acetate at 4 °C for 1 h. Finally, the cells were embedded into Spurr resin and left to polymerize in an oven at 60 °C for 24 h. Resins were sectioned by cutting an 80 nm film at 25 °C using an ultramicrotome Buehler ISOMET. The grids were examined using a JEOL–JEM 1200EXII electron microscope. For SEM micrographs; a drop of the suspension of collected cells by centrifugation was deposited onto a gold-coated glass slide and air-dried before the image collection.

Results and discussion

TEM micrograph of colloidal Cu nps was obtained at bright field. The particle size is represented by a histogram, to calculate the size distribution and normal deviation, as shown in Fig. 1a. The measurement of the particle size was randomly chosen, 100 particles were counted in the micrograph in order to estimate the average size. Therefore, the mean particle size of colloidal Cu nps obtained by normal curve fit is 10.6 ± 1 nm. Histogram was obtained using the software Origin 6.0 [14] which gives information about the particle size.

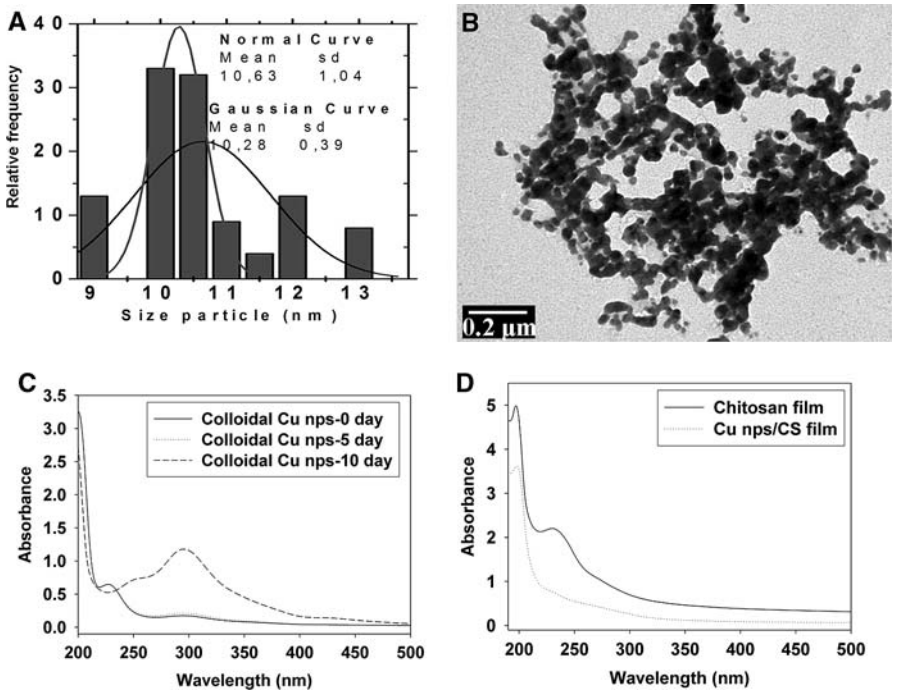

Fig. 1 **a** Particle size distribution of colloidal Cu nps, **b** TEM micrograph of colloidal Cu nps, **c** UV–vis spectra of colloidal Cu nps, **d** UV–vis spectra of films

Colloidal Cu nps showed an absorption maximum in UV spectra at 230 nm from 0 to 5 days (Fig. 1c). Cu nps agglomeration at 10 days exhibited a shift to 300 nm, which corresponds to particle growth. The UV–visible spectra of the composite film (Fig. 1d) revealed two absorption peaks at 200 nm corresponding to the absorption of chitosan and to 230 corresponding to colloidal Cu nps. Colloidal Cu nps were easily incorporated in chitosan solution, possibly due to electrostatic interactions, produced by cationic nature of chitosan solutions and oxygen free electrons of 2-propanol. Also, hydrogen bonding and hydrophilicity of chitosan is an appropriated characteristic for colloidal Cu nps incorporation. Colloidal Cu nps are blended into a chitosan matrix achieving an excellent dispersion, which suggest that the colloidal Cu nps are effectively wetted by the chitosan solution. Visual physical appearance of both films such as brittleness, flexibility, smooth surface, lamination, toughness was not different. Both films were homogenous, easy to handle and were not sticky.

Medium FTIR spectrum of composite film is mostly similar to the CS film (Fig. 2a). Bands attributed to –OH and $–NH_2$ stretching groups are shifted to low frequency for films respect to CS powder (with and without colloidal particles), due to alcohol and carboxylate, respectively. Bands attributed to C=O stretch (amide II) are shifted to significant higher frequency respect to chitosan powder, possibly by acetate presence. Important evidence of N–Cu interaction [15] and Cu–O [16] can be observed in far FT-IR spectra. Table 1 summarizes the absorption bands of medium and far FTIR spectra.

Table 2 summarizes the thermal behavior of films. The first thermal step was related to water evaporation and residual 2-propanol present in composite film. It is noteworthy that colloidal Cu nps decrease the T_{d1} when is compared to chitosan film. The interaction of many OH hydrophilic groups of the chitosan with OH groups and Cu^{2+} ions of colloidal Cu nps is the main reason for low moisture content of this composite film. Second thermal step started over 170 °C and was related to acetate loss of chitosan salt for both films. Probably, the weight loss in composite film is higher because of the oxidation of glucosamine to glucosamine acid produced by colloidal Cu nps at high temperature [17], resulting in the formation of H_2O and CO_2. The third step started over 250 °C, and was related to depolymerization of glucosamine chains. All films showed a decrease of

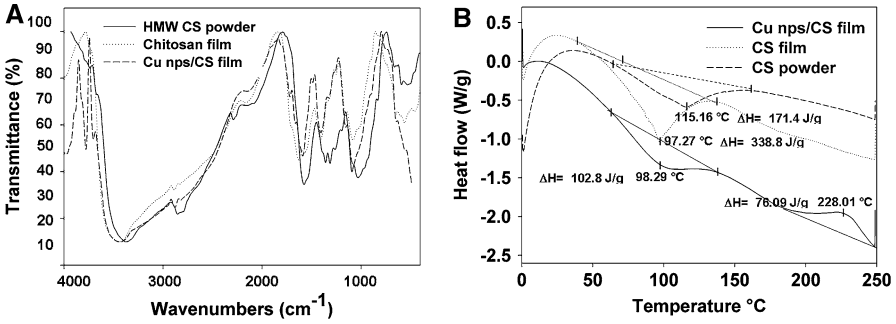

Fig. 2 **a** Characteristic absorption bands in infrared spectra and **b** DSC curves

Table 1 Characteristic absorption bands (cm^{-1}) in infrared spectra

Assignment	Chitosan powder	CS film	Cu nps/CS film
–OH and $–NH_2$ axial stretch	3,445.18	3,433.59	3,431.03
−C–H axial stretch	2,920.77	2,942.25	2,879.33
C=O stretch (amide II)	1,519.34	1,557.38	1,589.11
Coupling of C–N axial stretching	1,425.88	–	–
Coupling of C–O axial stretching	–	1,412.21	1,406.22
N–H angular deformation	1,380.77	1,320.58	1,323.62
Polysaccharide skeleton (glycosidic bonds, C–O and C–O–C stretching)	1,097.94	1,079.60	1,079.58
δ (CH) or ρ_r(COO)	356.29	453.05	437.38
ν(Cu–O)	–	–	515.8
ν(Cu–N	–	–	442.1

Table 2 Thermal behavior of CS powder and films

Sample	T_{d1} (°C)	Weight loss (%)	T_{d2} (°C)	Weight loss (%)	T_{d3} (°C)	Weight loss (%)
HMW CS powder	87.5	6.9	–	–	352.4	50.3
CS film	141.0	17.0	209.4	8.7	319.7	38.1
Cu nps/CS film	87.5	8.8	218.8	9.7	314.7	41.1

temperature of glucosamine chains decomposition in contrast to T_{d3} of chitosan powder due to the loss of interpolymer chain interactions in film formation.

HMW chitosan powder shown two thermal events, the first attributed to moisture and the second attributed to glucosamine chains decomposition.

On the other hand, the colloidal Cu nps could contribute to the oxidation of glucosamine chains of film matrix during aging, favoring their degradation.

The DSC curves of films are shown in Fig. 2b. Initial endotherm shifted to lower temperature respect to CS powder for both films occurred over a temperature range (70–140 °C). This endotherm is attributable to water loss and represents the required energy to vaporize the water present in the samples. The moisture-retentivity of CS film was affected by the addition of colloidal Cu nps. The required energy of composite film is much lower, probably, because of the loss of the hydrogen bonding caused by sterical impediment of colloidal Cu nps.

The composite film showed a weaker exotherm at 228 °C respect to CS film. This transition corresponds, probably to residual acetate loss, dehydration, and pyrolitic decomposition of residual 2-propanol, resulting in the formation of H_2O, CO_2 and CH_4.

The hygroscopic nature of chitosan is a factor that affects several properties of films, such as permeability, thickness and stability. In general, carbohydrates films are ineffective water vapor barriers due to their high hydrophilicity. Chitosan films have a higher affinity for water because of the protonated chitosan molecules,

Table 3 Barrier properties of films

Sample	Metal content (%)	Thickness (mm)	WVP (g mm/m^2 day kPa)	OP (cm^3 mm/m^2 day kPa)	EMC (%)
Cs film	–	0.046 ± 0.007	3.0×10^{-3}± 0.001	0.17 ± 0.02	33.7 ± 1.7
Cu nps/CS film	0.17 ± 0.01	0.053 ± 0.004	3.3×10^{-4} ± 0.001	0.08 ± 0.01	6.1 ± 2.2

Table 4 Roughness of CS film and composite film

Films	Section	Rms (nm)	Ra (nm)	Rmax (nm)
Chitosan film	1st region	2.106	1.692	10.036
	2nd region	3.487	2.853	14.693
	3rd region	4.517	3.268	18.328
Cu nps/CS film	1st region	18.404	15.654	57.296
	2nd region	10.391	6.117	36.496
	3rd region	13.657	9.137	39.191

rendering the films more hydrophilic than the powder. Films properties can be compared in Table 3. Composite film, containing colloidal Cu nps at levels of 0.17%, increased the thickness of chitosan film in 15%. CS films showed higher WVP, respect to composite film. WVP is a very important parameter to consider; because the mechanism of water vapors permeation involves dissolution and further diffusion of components from matrix. Colloidal Cu nps decrease the water vapor permeability, increasing the resistance toward water. Possibly, there are three factors responsible for decreasing of water vapor permeability in composite film: (1) Hydrogen bonding interaction between chitosan and solvatation sphere, avoiding the availability of hydroxyl groups of chitosan in order to form bonds with water, (2) alcohol content, which increases the macromolecular mobility of the matrix and (3) roughness increase the tortuosity of the diffusion pathway, affecting consequently the permeability (Table 4).

The main difficulty for the use of colloidal Cu nanoparticles arises from their instability in air. Several factors affect the OP of films, such as physical state of additive, molecular weight, altered film structure due to chemical interaction of additive, and absorption of oxygen molecule. OP values decreased with colloidal Cu nps, probably due to a significant increase in the crystalline space produced by alcohol molecules of colloidal solvatation sphere. Colloidal Cu nps act as a bulky side group, decreasing the diffusion through the matrix, by restriction of O_2 flow. Equilibrium moisture content (EMC) is according with the first thermal event in TGA with losses of 8.8 and 17% for composite films and CS films, respectively. Composite film presented lower moisture content than CS films due to the volume of colloidal solution used for its preparation. Addition of metallic nanoparticles could facilitate the elimination of unbound water during microwave heating because of binding to biopolymer matrix by ion-dipoles or dipole-dipole, decreasing the

selectivity of film toward water. EMC gives an idea of initial water content of films and effectiveness of water elimination by microwave heating, significant parameters for the oxidation control of metallic nanoparticles.

Figure 3a and b show the thin section micrograph of the composite film. There are diffuse isolated metal particles separated from one another and dispersed as a monolayer. In the composite film, the colloidal Cu nps are coated with a thin layer of chitosan, then the van der Waals influence from the colloidal Cu nps can be masked, and this prevents the strong agglomeration of particles. Metal-free region

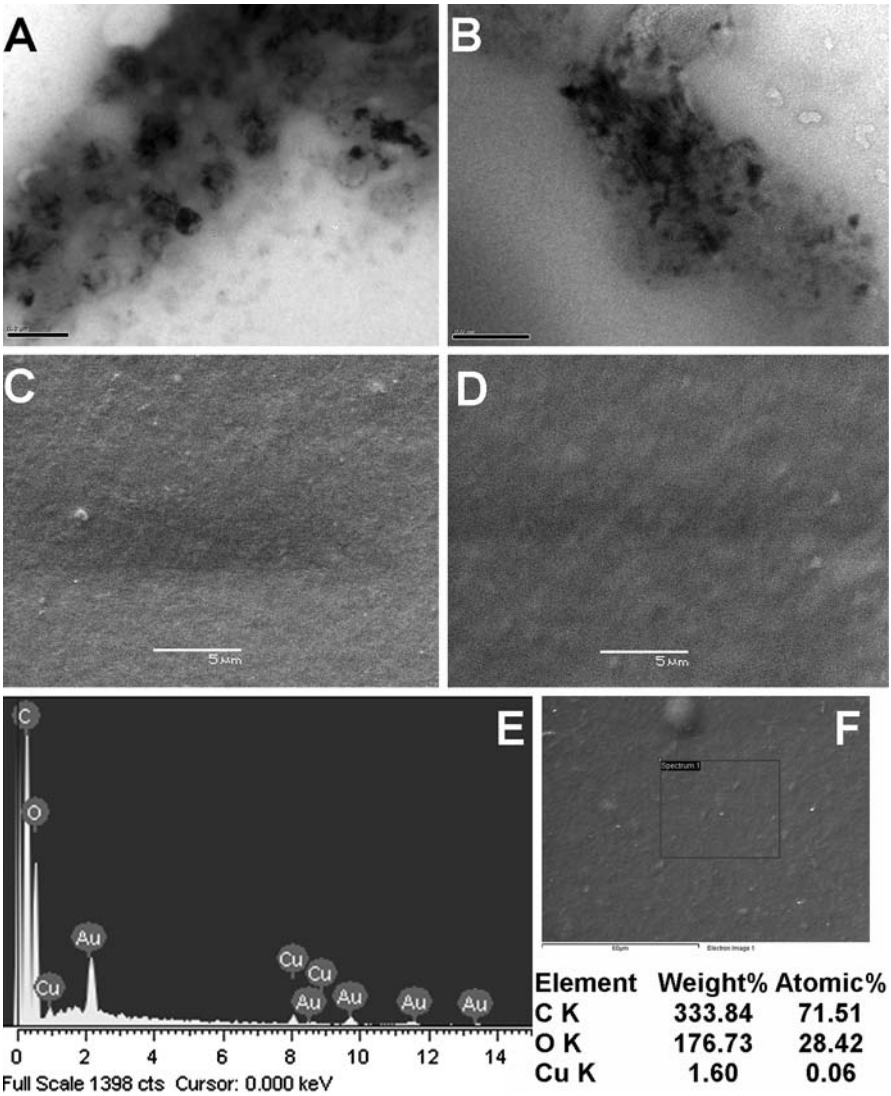

Fig. 3 **a** and **b** TEM micrographs (*thin section*) of composite film, **c** SEM micrograph of CS film, **d** SEM micrograph of composite film, **e** and **f** EDS spectrum for composite film and selected area of analysis

belongs to epoxy resin. The surfaces of both films were found to be smooth and homogenous as visualized by SEM micrographs (Fig. 3c, d). Micrographs revealed no cracks, no protuberances and no cavities in both films, general characteristic observed in CS films by additives addition [18]. Energy-dispersive spectrum showed that the major elements of film consisted of carbon (C), oxygen (O), and copper (Cu) (Fig. 3e). The atom number ratio of O/Cu was about 4.7.

AFM was used to characterize the surface topographic feature of film. The AFM images of films were shown in Fig. 4. Outer surface of CS film for Rms and Ra increases from 3.370 nm and 2.604 to 14.151 nm and 10.303 nm with the incorporation of colloidal Cu nps on the film. Colloidal Cu nps are immobilized in the film and thus prevent it from growing bigger; therefore composite film surface is rougher than CS film, with small patches of particles. Metallic nanoparticles introduced by electrostatic attraction in chitosan matrix reflected localized interconnection along polymer strands. On the other hand, the surface of CS film was smoother than composite film, without pores or cracks. Continuous profile

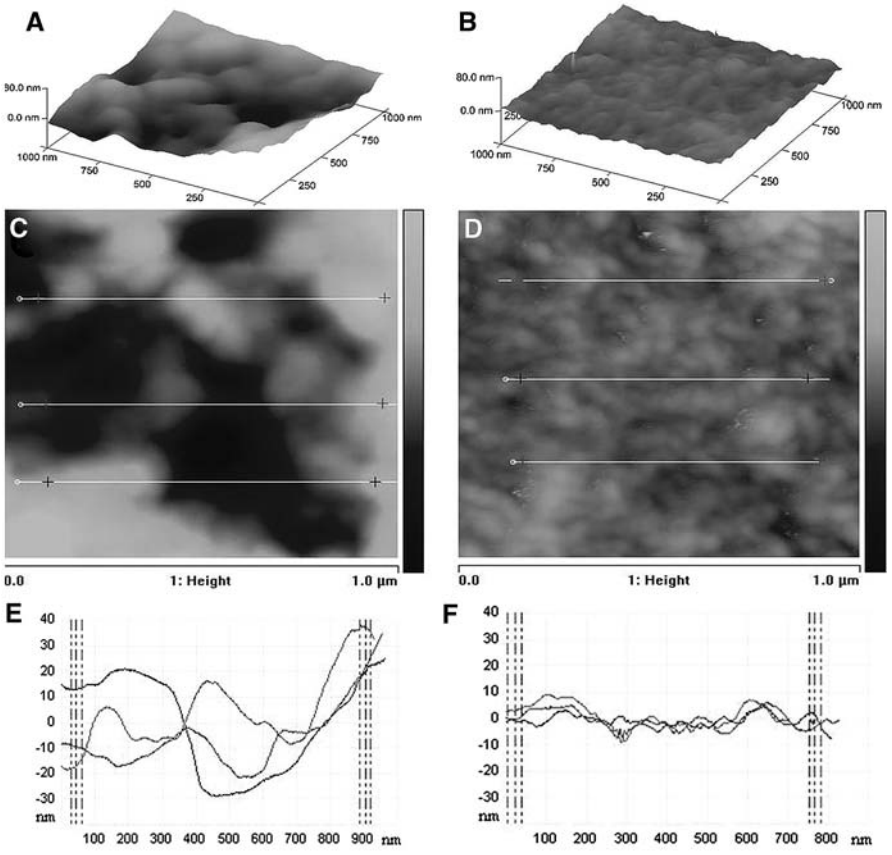

Fig. 4 AFM images of films. **a** Composite film, **b** CS film, **c** and **d** Lines roughness of three cross-sections of analysis, for composite and chitosan films, respectively, **e** and **f** Roughness sections profiles showing peak-to-valley height in line roughness for composite and chitosan films, respectively

corresponds to a network structure consisting mostly of chitosan. Figure 4a and b represent typical 3D surfaces, C and D displays the surfaces topography with cross-sections of films. Figure 4e and f show the cross-section profile and peak-to-valley height differences for the large features in the cross-section. From these figures, it is possible to observe a non-uniform distribution of colloid particles in cross-sections. Roughness may be ascribed to the spherical structure of colloidal Cu nps and certain level of agglomeration of particles during the preparation of film.

Composite film showed good barrier properties to UV light with a strong absorption of UV-C and UV-B light (200–350 nm), covering more UV region than CS film, as shown in Fig. 5a. CS film showed very high transparency in the visible region of the spectra (400–700 nm). Opacity may be affected by thickness, storage and film composition. Variation of opacity through 28 days of storage was no significant for both films (Fig. 5b). Figure 5c and d shows the transparency values along of UV-vis spectra for both films. In the visible range, composite film showed lower transparency than CS film.

The composite film was effective in reducing microbial concentration in the bulk fluid for both food-related microorganisms tested (Table 5). Viability mapping by electron microscopic examinations permitted to analyze the morphologic defects of *S. aureus* occurring in the presence of composite film.

Cell wall deformation is related to the cytoplasmic volume decrease (Fig. 6b) and the detrimental structural change is the result of the cell shrinkage. TEM images

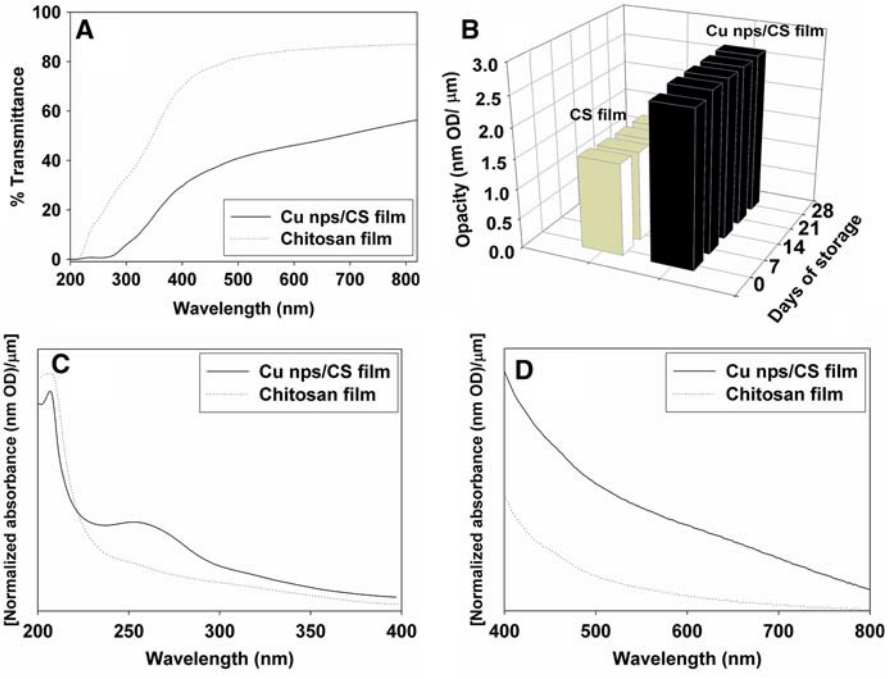

Fig. 5 **a** UV–vis transmittance spectra of films, **b** variation of opacity along storage, **c** transparency of films in UV range and **d** transparency of films in vis range

Table 5 Reduction of microbial concentration in the liquid culture exposed to films

Bacteria	Chitosan film		Composite film	
	Initial concentration (cells/ml)	Final concentration (cells/ml)	Initial concentration (cells/ml)	Final concentration (cells/ml)
S. aureus	3.3×10^6	3.0×10^5	3.3×10^6	1.0×10^2
S. Typhimurium	3.3×10^6	1.8×10^5	3.3×10^6	2.1×10^3

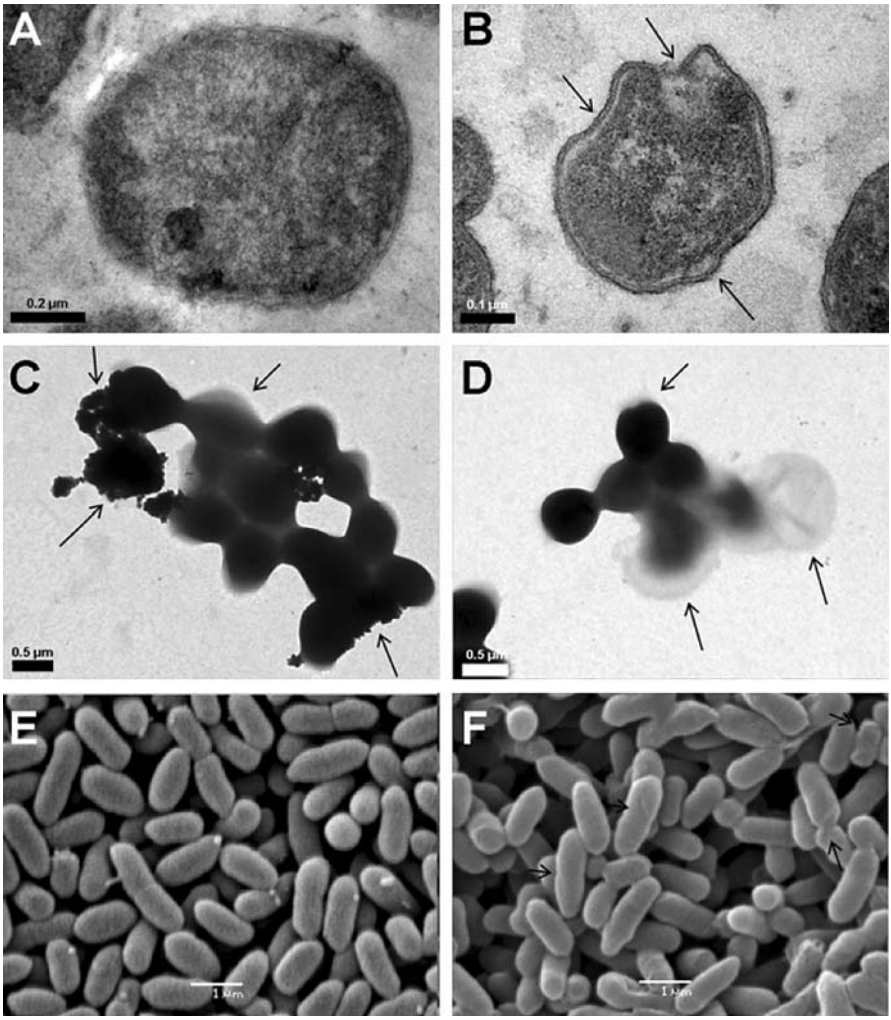

Fig. 6 **a** TEM micrograph of thin section of untreated *S. aureus,* **b** TEM micrograph of thin section of *S. aureus* treated with composite film, **c** and **d** TEM micrograph of deposition onto copper grid of *S. aureus* treated with composite film, **e** SEM micrograph of untreated *S.* Typhimurium and **f** SEM micrograph of *S.* Typhimurium treated with composite film

acquired from liquid cultures shown disintegration of cell wall. This perturbation takes place as perforation of the peripheral wall (Fig. 6c, d), increasing the cell stress by the internal turgor with release of intracellular material. As shown in the Fig. 6e, cell wall of *S.* Typhimurium is very rough due to the cell wall components, which are also possibly crosslinked, resulting in heterogeneous surfaces. Treated cells with composite film appeared smooth, collapsed, cracked and markedly shrank as shown by the arrows (Fig. 6f). Another morphological alteration was the appearance of blebs seemed to be derived from the cell wall.

Conclusions

A film based on chitosan and colloidal Cu nps was successfully prepared by casting technique with microwave heating. CLD method gives an appropriate nanoparticle size for its inclusion in chitosan matrix. The film-forming solution exhibited good dispersion and film-forming property due to the high density of amino and hydroxyl groups of chitosan, avoiding the aggregation of metallic particles. Barrier properties of composite film and chitosan film were investigated; the results demonstrated that composite film showed advantages over chitosan film in oxygen permeability, water vapor permeability and light transmission. Further studies in terms of metal concentration are needed to increase the antimicrobial activity of films. Information from this study can be employed in guiding futures strategies for the study of composite films that could be used to protect food and extend their shelf life.

Acknowledgments We are grateful to Agencia Chilena de Cooperación Internacional (AGCI), Comisión Nacional de Investigación en Ciencia y Tecnología (CONICYT, AT-24071064; 21050655) and Centro de Investigación de Polímeros Avanzados (CIPA) for scholarship grants. Sincere thanks are also given to FONDECYT 1080704, Mecesup (Beca de estadía en Centros de investigación en el extranjero) and Serveis Cientificotècnics, of the Universitat de Barcelona for the use of the equipments.

References

1. Kickelbick G (2006) Hybrid materials: synthesis, characterization and applications. Wiley-VCH, Weinheim, pp 1–13
2. Meléndrez MF, Díaz J, Cruzat C, Arbiol J, Cárdenas G (2009) Synthesis and aggregation study of tin nanoparticles and colloids obtained by chemical liquid deposition. Colloid Polym Sci 287:13–22
3. Cárdenas G, Vera V, Muñoz C (1998) Silver colloids from nonaqueous solvents. Mater Res Bull 33:645–653
4. Muzzarelli R, Isolati A, Ferrero A (1974) Chitosan membranes: ion exchange and membranes, vol 1. Gordon and Breach, London, pp 193–196
5. Gontard N, Guilbert S, Cuq JL (1993) Edible composite films of wheat gluten and lipids: water vapour permeability and other physical properties. J Food Sci 58:206–211
6. McHugh TH, Avena-Bustillos R, Krochta JM (1993) Hydrophilic edible films: modified procedure for water permeability and explanation of thickness effects. J Food Sci 58(4):899–903
7. McHugh TH, Krochta JM (1994) Water vapor permeability properties of edible whey protein–lipid emulsion films. J Am Oil Chem Soc 71:307–312
8. Shellhammer TH, Krochta JM (1997) Whey protein emulsion film performance as affected by lipid type and amount. J Food Sci 62:390–394
9. Cárdenas G, Díaz J, Meléndrez MF, Cruzat C (2008) Physicochemical properties of edible films from chitosan composites obtained by microwave heating. Polymer Bull 61:737–748

10. Lima CAS, Oliva R, Cárdenas G, Silva EN, Miranda LCM (2001) Influence of the thermal annealing on the electrical resistivity and thermal diffusivity of Pd:Ag nanocomposites. Mater Lett 51:357–362
11. ISO (1995) Sheet materials. Determination of water vapour transmission rate. Gravimetric (dish) method. ISO 2528. In: ISO/TC 6: Paper, board and pulps, SC 2: Test methods and quality specifications for paper and board, Geneva, Switzerland
12. Pinotti A, García MA, Martino MN, Zaritzky NE (2007) Study on microstructure and physical properties of composite films based on chitosan and methylcellulose. Food Hydrocoll 21:66–72
13. Cho SY, Rhee C (2004) Mechanical properties and water vapor permeability of edible films made from fractionated soy proteins with ultrafiltration. LWT 37(8):833–839
14. Origin 6.0 Microcal ^{TM} Microcal Software, Inc.
15. Kobayashi Y, Sakuraba T (2008) Silica-coating of metallic copper nanoparticles in aqueous solution. Coll Surf A: Physicochem Eng Asp 317:756–759
16. Nakamoto K (1977) Infrared and Raman spectra of inorganic and coordination compounds, 3rd edn. Wiley, Inc, London
17. Sun C, Qu R, Chen R, Ji C, Wang C, Sun Y, Wang B (2008) Degradation behavior of chitosan chains in the 'green' synthesis of gold nanoparticles. Carbohydr Res 343:2595–2599
18. Wang X, Du Y, Luo J, Lin B, Kennedy JF (2007) Chitosan/organic rectorite nanocomposite films: structure, characteristic and drug delivery behavior. Carbohydr Polym 69(1):41–49